Time/frequency analysis of contact-friction instabilities. Application to automotive brake squeal.

G. Vermot des Roches[1,2], **E. Balmes**[1,3], **T. Pasquet**[4], **R. Lemaire**[4]
[1] Ecole Centrale Paris, Laboratoire MSS-MAT, CNRS UMR 8579
Grande Voie des Vignes, 92295, Chatenay-Malabry, France
[2] SDTools
44, Rue Vergniaud, 75013, Paris, France
vermot@sdtools.com balmes@sdtools.com
[3] Arts et Metiers ParisTech, Laboratoire PIMM (SDS), CNRS UMR 8006
151, boulevard de l'hôpital, 75013, Paris, France
[4] Bosch (Chassis Systems Brakes),
126, Rue de Stalingrad, 93700, Drancy, France
Thierry.Pasquet@fr.bosch.com Remi.Lemaire@fr.bosch.com

Abstract
Robust design of silent brakes is a current industrial challenge. Braking systems enter in the more general context of unstable systems featuring contact friction interaction. Their simulation requires time integration schemes usually not adapted to combination of large industrial models (over 600,000 DOF) and long simulations (over 150,000 time steps). The paper first discusses selection of the contact/friction model and adaptations of the integration scheme. The relation between the nominal steady state tangent modes and the system evolution over time is then evaluated. The time response shows a nearly periodic response that is analyzed as a limit cycle. It is shown that instantaneous *dynamic* stability predictions show stable/unstable transitions due to changes in the contact/friction state. These transitions are thought to give an understanding of the mechanism that limits levels for these self sustained vibrations. The concept is exploited to suggest novel ways to analyze complex modes.

Introduction

Optimized weight/performance nowadays considered in automotive brake design tends to generate noisy systems. High friction coupling happening at the pad/disc interface is responsible for self-sustained vibrations in the audible frequency range, known as *squeal* between 1 and 16 kHz or *moan* under 1kHz. Noise levels can reach 120dB in the brake vicinity. Squeal, being a high frequency vibration, does not alter brake performance and happens mostly at low pressure, low speed conditions. The nuisance is however strong for the driver and environment and tends to alter the perceived quality.

Classical design methods [1, 2] for brake vibrations are frequency based. The system is linearized around a static operation condition and the real part of complex eigenvalues are studied following Lyapunov's theorem. This method however tends to present more unstable modes than really found experimentally and does not provide mechanisms to classify those that are really going to respond or to evaluate actual vibration levels.

These limitations motivate the use of time domain simulations. Implementation is however a major challenge since a straight forward simulation for a full industrial model has prohibitive computational costs. Contact handling requires relatively small time steps around $10^{-6}s$ which makes long (100ms) simulations difficult to handle. Using a non linear implicit Newmark scheme on a 600,000 DOF system would actually generate over 1TB of data in over 700 hours. To address the problem, adapted contact-friction formulations are discussed in

section 1, a model reduction technique is presented in section 2.1 and an adaptation of the Newmark scheme to non linear penalized contact is presented in section 2.2. The simulation cost then becomes affordable yielding from 500MB to 5GB of data in 12 hours. Work on initial states can then improve performance for design phases.

Applications to the simulations of a real brake are then discussed in section 3. The classical stability diagram for a static state is shown and the transient analysis is shown to lead to a bounded nearly periodic response that is taken to be a *limit cycle*. Modal energies are shown to present significant oscillations during this cycle so that the notion of an underlying linear model, necessary to define modes, does not seem appropriate. It is thus proposed to compute stability diagrams at various points during the cycle. This novel analysis shows that the system is stable during a significant fraction of the cycle and that strong mode coupling occurs. The analysis seems quite adapted to help designers and a new strategy to evaluate complex modes of the system linearized around its static state is proposed in section 3.3.

1 Contact formulation

1.1 Model choices

Contact/friction modeling is commonly split into two formulation strategies. Contact can either be formulated as a structural constraint using a Lagrange formulation, or regularized using a penalized formulation. Numerically, these strategies are handled differently.

Both formulations are based on the gap between a set of contact points selected at the interface. Practically, the gap between two surfaces is defined as the relative displacement along the contact normal N with a possible offset g_0, as

$$\{g\} = N.(u_{slave} - u_{master}) - \{g_0\} \tag{1}$$

A slave/master strategy is commonly employed, so that a set of contact points is defined on the master surface from which distances are computed regarding the facing slave surface. These strategies are well documented, for example in the ABAQUS manuals [3].

Contact implementation follows the definition of the Signorini contact law, for a gap between two solids (defined as positive when contact is open) and the resulting contact pressure p states the relation

$$\begin{cases} g \geq 0 \\ p \geq 0 \\ (g).(p) = 0 \end{cases} \tag{2}$$

This ideal formulation, plotted in figure 1a excludes solid interpenetration at the contact points, and imposes null repulsive contact forces if the contact is opened.

The resolution of such system of equation requires to keep the contact forces as unknowns. Hence the use of a Lagrangian method to resolve a coupled displacement/contact constraint problem. Interactions with the time integration scheme tend to occur as detailed in section 2.2.

Penalization methods relax the contact constraint induced by equation (2) by authorizing a controlled level of interpenetration. Practically, a relationship between the gap and contact forces is established to account for an approximated contact constraint. The result is another ideal approximation of real contact laws, that is not necessarily less valid than Signorini. Indeed, the reality of contact between rough surfaces lies in the local compression of asperities. Such compression can imply at the global level an interpenetration of the mean surfaces corresponding to the finite element mesh.

Figure 1a plots several adapted formulations of penalized contact laws. The contact law retained by Bosch is of the exponential type defined at each contact point by

$$p(g) = p_0 e^{-\lambda g} \tag{3}$$

where p_0 and λ are constant parameters, to be determined potentially experimentally. With such contact law the non linear problem can be formulated with displacement dependent non linear forces.

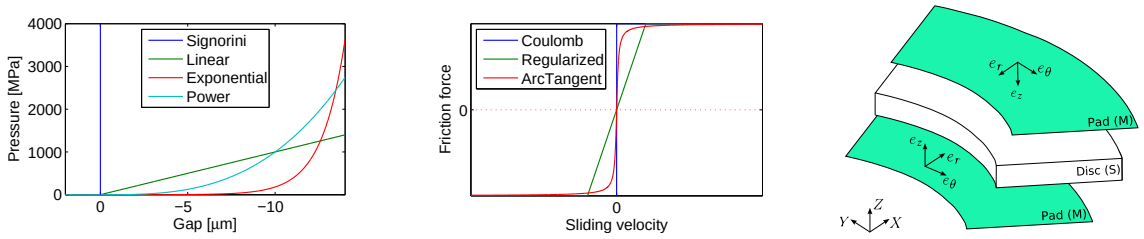

(a) Contact models (b) Friction models (c) Local cylindrical frame

Figure 1: Contact/Friction models and local frame definition of the pad/disc contact

Friction implementation follows Coulomb's law, which for two solids relates the sliding velocity w_s and friction forces F_T, through

$$\begin{cases} \|F_T\| \leq \mu \|F_N\| & w_s = 0 \\ \|F_T\| = \mu \|F_N\| & \exists A \geq 0, w_s = -AF_T \end{cases} \tag{4}$$

This ideal formulation plotted in figure 1b requires sticking states (zero sliding velocity) to be solved through the use of constraints. Augmented Lagrange methods allows a complete resolution of a coupled velocity/friction force problem. As for contact laws, relaxation techniques can be applied such that a determined relationship exists between the sliding velocity w_s and the local friction forces F_T, depending on the normal contact force F_N and the friction coefficient μ.

A basic regularization, plotted in figure 1b and considered in the study, penalizes low sliding velocities through the introduction of a parameter k_t, such that

$$\begin{cases} \|F_T\| = k_t \|w_s\| & \text{if } \|w_s\| < \frac{\mu}{k_t} \|F_N\| \\ \|F_T\| = \mu \|F_N\| & \text{else} \end{cases} \tag{5}$$

The numerical behavior of such model is questionable regarding non sliding states. Richer analytical models are of interest as a perspective for the present study. Dahl friction models [4, 5] thus introduce an hysteresis formulation better approaching non sliding states.

If not using richer models, it may be interesting to use a continuously derivable analytical formulation of the friction law to avoid numerical pathologies. Indeed, the integration scheme applied in section 2.2 assumes a good regularity of the model. To this effect an Arctangent function can be used as a friction law and is plotted in figure 1b.

1.2 Numerical implementation

In application of the finite element method, the strategy chosen here takes the master contact points at the gauss integration points of the surface elements associated with the friction pad volume. The gap defined in equation (1) is then evaluated by computing weighted distances between the gauss contact points of the master surface and its projection on the slave surface by a classical finite element interpolation. The gap is then formulated with an observation matrix $[C_{NOR}]$

$$\{g\} = [C_{NOR}] \{q(u)\} - \{g_0\} \tag{6}$$

The force resulting from the contact pressures of equation (3), with the gap defined at each gauss point by equation (6), is then defined as

$$\{\hat{q}\}^T \{f_N\} = \int \{\hat{u}(\hat{q})\}^T N p dS \simeq \sum_j \{\hat{u}(\hat{q})\}^T \{N\} p(x_j, q) \omega_j J(x_j) \tag{7}$$

where f_N is the global contact force, p the contact pressure (from equation (3)), x_j are the integration points, $\hat{q}$ a virtual displacement, q the displacement, $J(x_j)$ the Jacobian of the shape transformation (surface associated to each integration point) and ω_j the weighting associated with the integration rule.

A similar operation can be performed on the tangential direction to determine the sliding velocity, namely w_s as function of the system velocity $\dot{q}$, through the use of an observation matrix of relative tangential displacement $[C_{TAN}]$

$$\{w_s\} = [C_{TAN}] \{\dot{q}\} \tag{8}$$

$[C_{TAN}]$ is constructed as $[C_{NOR}]$ for tangent directions.

The pairing operation matches the set of master contact points to the slave surface. Due to the number of contact points, it is computationally very costly. Pairing is therefore performed only once by computing contact forces in a local rotating frame, plotted in figure 1c. Friction is only considered along tangential (e_θ) direction. Implementation details can be found in [6], in which the resulting *Eulerian*-like formulation is developed, yielding the following expression of the sliding velocity,

$$\{w_s\} = [C_{TAN}] \{\dot{q}\} + \{\Omega_{disc}\} \wedge \{r(q)\} + \{\Omega\} q(u_\theta)_{,\theta} \tag{9}$$

In addition to the local sliding velocity, the disc rotation (a constant depending on the geometric position of the contact point) and a tangential convection term (obtained through another observation matrix) are added. Due to the low disc rotation speed (a few rad/s), higher order terms such as the gyroscopic effect are neglected.

1.3 Notion of tangent contact-friction states

1.3.1 Introduction

The contact non-linearity presented in section 1.2 is treated in transient analysis as non linear loads added to the mechanical equilibrium equation

$$M\ddot{q} + C\dot{q} + K_0 q = f_{ext} + f_N(q) + f_T(q, \dot{q}) = f_{ext} + f_{int}(q) = f_{ext} - K_{nl}(q) q \tag{10}$$

where K_0 is the system elastic stiffness without non linear effects. Time simulations directly compute the contact forces in the residue.

As suggested in equation (10), the contact forces considered are internal to the system studied, so that equation (10) can be rewritten through the use of a non-linear stiffness $K_{nl}(q)$matrix relating f_{int} and q. Using such formalism raises issues regarding the definition of the system modes in a clear way. Modal computations are performed for linear models, computation of non-linear complex modes is possible [7, 8] yet difficult to exploit for industrial models.

The most common approach is to consider the system linearized around a deformation state and compute the modes of the linearized system. The linearized model is then called *tangent* to the said deformation state. This strategy is of course limited as linearizing in the vicinity of deformation states can only be relevant for very small deformation deviations from the chosen working point.

1.3.2 Tangent contact

Depending on the chosen contact formulation, the expression of the system linearization varies a lot. Considering a Lagrangian formulation, the definition of the tangent state only depends on the surface effectively in contact, as a contact point is either *open* (no contact) or *closed* (in contact). The open case generates then no contact stiffness, while the closed case generates an exact continuity constraint for the normal displacement at the interface.

Penalized contact formulations are defined as function of the gap, such that a tangent state can be derived for each contact point depending on its penetration level. For the exponential contact law used in this paper, at a given contact point i, the contact stiffness k_{ci} is defined by the derivative of equation (3)

$$k_{ci}(q) = \frac{\partial p_i(q)}{\partial q} = -p_0 \lambda e^{-\lambda g_i} \tag{11}$$

where g_i is the gap at a contact point i observed at the i^{th} line of the gap observation matrix $[C_{NOR}]$.

The tangent contact stiffness matrix $K_{nlc}(q)$ is then recovered by the gap observation matrix, such that

$$K_{nlc}(q) = [C_{NOR}]^T \left[\backslash k_{ci}(q) \backslash \right] [C_{NOR}] \tag{12}$$

The effect on the system itself is a perceived stiffness variation occurring at the contacting interfaces. Linearization of the contact state is locally performed for each contact point separately. For large vibrating 3D interfaces the distribution of contact stiffness can then show large variations over the surface, as will be illustrated in section 3.2.

1.3.3 Tangent friction

Based on equation (10), a tangent friction state should be added to the system. Its definition is rather peculiar as it can be non symmetric – it is after all the only instability source for the squeal simulations presented in section 3. The nature of friction as written in equation (4) shows that a variation of contact force has a direct effect on friction force, while a variation of the friction force may occur without effect on the contact force. This non symmetric notion is illustrated in figure 2 where stiffness coupling matrix topologies are illustrated for a basic case. Computing real modes requires symmetric positive definite matrices thus needing a proper definition of friction handling.

A contact point is either *sticking* ($w_s = 0$) or *sliding* ($w_s \neq 0$). For both Lagrangian and regularized formulations, the same approach can be used. In the case of a sliding state, the friction force is explicitly defined and only depends on the contact force at the same point. The tangent friction is then the tangent contact (11) scaled by the friction coefficient μ, linking the normal and tangent displacements for complex modes. For real mode computation, since the tangent displacement is free for a fixed contact state, no stiffness is added. The tangent friction coupling stiffness K_{nlf}^{slide} for sliding states is defined as

$$K_{nlf}^{slide} = \begin{cases} 0 & \text{for real mode computation} \\ [C_{TAN}]^T \left[\backslash \mu k_{ci}(q) \backslash \right] [C_{NOR}] & \text{for complex mode computation} \end{cases} \tag{13}$$

In application to brake squeal, the pad/disc contact is sliding, such that the definition from equation (13) can be sufficient. A full brake assembly is however considered in this article, which model features 8 components in non linear contact interaction before reduction (section 2.1). The other components are sticking together at the steady state so that tangent friction coupling stiffness for sticking contact states must be addressed.

For sticking contact points, the basic Lagrangian approach will consider an exact continuity constraint of the tangential displacement at the interface, thus making it a bilateral constraint. Taking such pattern into account is critical for the complex modes as a physical resistance to the tangential displacement occurs.

A penalized approach can be used, which relaxes the Lagrange constraint. The friction force is however unknown inside the Coulomb cone, and further studies are necessary to characterize the stiffness coupling levels and the system sensitivity. Experiments are suggested in [9, 10] for non metallic materials.

The strategy chosen here is to consider the Coulomb cone limit characterized by the contact force level, such that the same tangent friction stiffness level $\mu k_{ci}(q)$ as for sliding states is used. The stiffness is overestimated, but will be close to microslip patterns which may occur for low vibration levels. It can be noticed that friction levels are lower in the other brake assembly interactions as metal/metal contact occurs ($0.1 < \mu < 0.3$).

The tangent friction coupling stiffness K_{nlf}^{stick} for sticking states is defined for both real and complex mode computations as

$$K_{nlf}^{stick}(q) = [C_{TAN}]^T \left[\backslash \mu k_{ci}(q) \backslash \right] [C_{TAN}] \tag{14}$$

To illustrate the effect of the different tangent contact-friction matrices presented here, an example based on a very simple problem is here presented. The basic model given in figure 2a features two cubes into vertical contact. For illustration purposes, the degrees of freedom (DOF) are segregated by their direction, 1 and 2 define the horizontal directions while 3 is the vertical normal direction, in which contact is is defined.

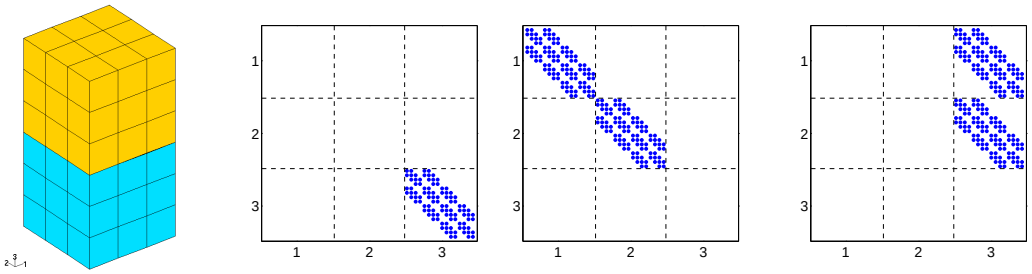

(a) Cube model (b) Contact (c) Sticking friction (d) Sliding friction

Figure 2: Tangent contact-friction matrix topologies on a simple case

Figure 2 presents the topologies of the tangent contact-friction matrices expressed on the master surface DOF. The tangent contact friction matrix (figure 2b) couples the normal direction, following equation (12), here identified to the third direction. The matrix is then symmetric positive definite and is used for real or complex mode computation.

The tangent friction matrix of equation (14) for sticking states in real and complex modes computation is plotted in figure 2c. It couples directions 1 and 2 independently and is symmetric positive definite.

The tangent friction matrix of equation (13) for sliding states in complex mode computation is plotted figure 2d. The unsymmetric coupling occurs as direction 3 is coupled to both directions 1 and 2 so that a deformation along 3 impacts directions 1 and 2 but not the other way around.

2 Time simulation of large finite element models showing local non-linearities

2.1 Model reduction

This section briefly presents the reduction method detailed in [11]. The aim is to generate an efficiently reduced model showing local non linearities. The reduced model must then be accurate (*i.e.* have exact real modes), of reasonable size, and with a reasonable matrix sparsity.

The presence of a local non linearity at the pad/disc interface drives the reduction strategy towards an hybrid superelement/FEM (Finite Element Model) coupling, as shown in figure 3. The pad lining material is deemed of importance as it is softer and will thus be proner to show wave propagation patterns through its thickness. The rest of the model is considered to behave linearly along the tangent deformation state corresponding to a steady state working point.

The area explicitly retained for the disc can be discussed and is either a section of the braking track, as presented in figure 3, or the DOF of the disc surface points in contact with the braking pad (which is preferred here). All DOF in the vicinity of the contact area are thus kept explicitly, noted q_c. The remaining of the system DOF are noted q_b.

To achieve the accuracy and sparsity objectives of exact dynamic behavior, one proposes a Rayleigh-Ritz method using the full system modes and the steady state response q_0 as assumed shapes. As only the q_b DOF will be reduced, the trace (or restriction) of the Rayleigh-Ritz basis on this part only is considered. The reduction basis, illustrated in figure 3, is then expressed as

$$\left\{ \begin{array}{c} q_b \\ q_c \end{array} \right\} = \left[\begin{array}{cc} [[\phi_{1:NM}]_b \ q_{0b}] & 0 \\ 0 & [I]_c \end{array} \right] \left\{ \begin{array}{c} q_r \\ q_c \end{array} \right\} \tag{15}$$

Such feature allows in particular to generate reduced models with exact real modes, as presented in [12].

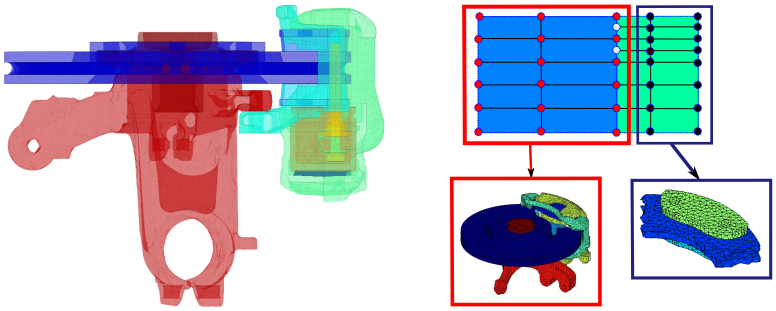

Figure 3: Left: View of the industrial brake model provided by Bosch. Right: Industrial brake model reduction strategy. The blue part is kept unreduced, the red part is reduced, also implicitly reducing the interface (red and green nodes)

The interface DOF between the superelement and the FEM are set in the superelement, so that they are implicitly reduced. The reduced matrices are consequently much sparser since the full coupling blocks usually produced by a Craig-Bampton reduction are avoided. To comply with the maximum frequency of interest (18kHz) 250 real modes need to be kept, so that the superelement size is 251×251. The reduced model used in further applications is of size 30,767 from the initial 600,000 DOF.

2.2 Time integration

A large number of schemes are available to perform numerical time integration. The most common methods come from the Newmark family which implementation is well documented [13]. The Newmark method cannot handle constraints properly [14, 15], which makes its use difficult for contact problems, especially when handled as a Lagrange constraint. The HHT-α method [13] implements acceptable numerical damping to handle numerical instabilities due to constraints, but not in a really convincing way [16].

Simulation of instabilities requires the use of a well controlled damping strategy [17]. Difficult to asses numerical damping implementations are avoided through the choice of an implicit non linear Newmark scheme [13] with coefficients set to $\beta = \frac{1}{4}$ and $\gamma = \frac{1}{2}$, presented in figure 4.

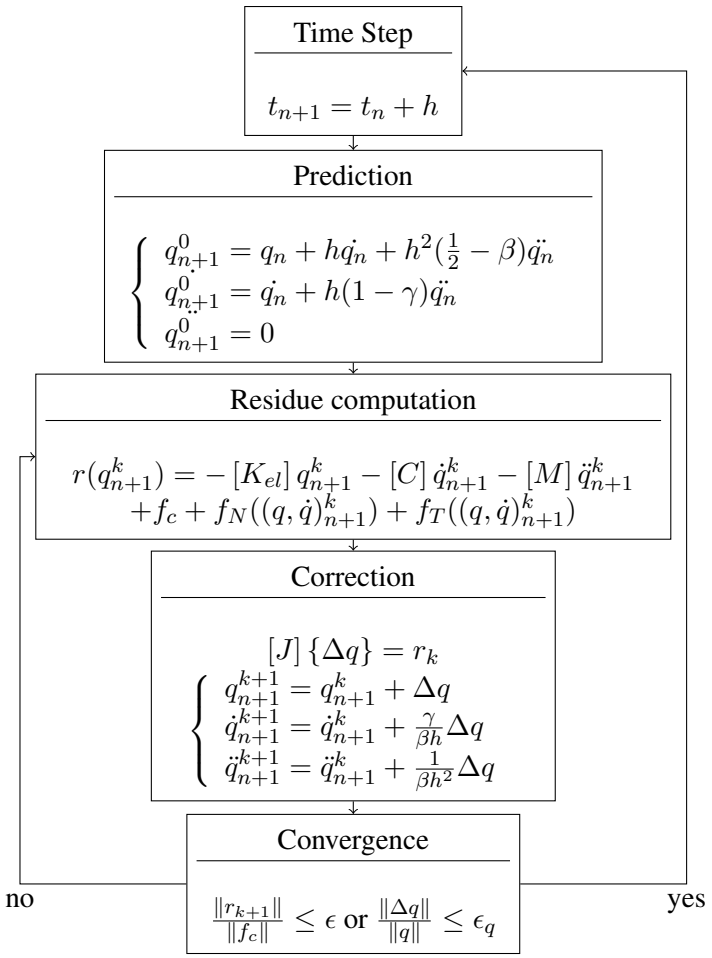

Figure 4: Implementation of the non linear modified Newmark scheme with condensed contact forces

High frequencies are handled by a global Rayleigh damping strategy. Setting the mass coefficient $\alpha_R = 0$ and the stiffness coefficient β_R very low ($\simeq 10^{-7}$) allows significant damping values at high frequencies only. The global Rayleigh is applied to the system assembled matrices as

$$[C_R] = \alpha_R\,[M] + \beta_R\,[K] \tag{16}$$

The implementation given in figure 4 and more detailed in [11], is adapted to the contact formulation, and to long time simulations (150,000 steps) of large problems (40,000 DOF). The ability to pass such computation in a reasonable amount of CPU time lies in the use of a fixed Jacobian. A classical Newmark scheme would recompute and factorize the Jacobian $[J]$ at each time step for each correction increment. The most efficient solvers still need around 10s to factorize a matrix of such size, which would take over 600 hours to perform, assuming one correction increment per time step.

To take contact forces into account, the Jacobian is set up with a mockup linear bilateral contact law which stiffness k_c is parametrized. The traditional Jacobian in the case where the non linearity only comes from contact friction is given in [13]. It is here modified as

$$[J] = \frac{1}{\beta h^2}[M] + \frac{\gamma}{\beta h}[C] + [K_0] + k_c\,[\mathsf{K_c}] \tag{17}$$

where $[\mathsf{K_c}] = [C_{NOR}]^T\,[C_{NOR}]$.

Further optimization concerns the adaptation of the convergence criterion, in conjunction with the time step. The larger the time step the larger the correction potentially needed, the more Newton-Raphson increments. Depending on the CPU time distribution between these tasks, an optimum balance between the number of time steps and the estimated Newton resolution has to be found.

3 Application to a realistic brake model

The realistic brake model provided by Bosch is shown in figure 3. It is simulated following the modeling strategies presented in sections 1 and 2. The study is set at a 12Bar braking pressure, and a disc velocity of $5rad/s$. These parameters were indicated by Bosch as prone to generate squeal on this particular model.

3.1 Instability characterization

The brake system is first simulated in the frequency and time domain to illustrate squeal triggering patterns and show the limitations of the classical tangent state only computation. To ascertain mode denomination, a prefix is added to the mode numbers such that the jth real mode is noted Rj, and the jth complex mode is noted Cj.

3.1.1 Stability derived from the steady state tangent state

The most common method nowadays used in the industry is based on the complex mode computation at the tangent state, as defined in section 1.3. The real brake features several unstable modes plotted in figure 5. In particular, 3 modes can be highlighted as significantly unstable, namely C44 (plotted in figure 5), C51 and C84.

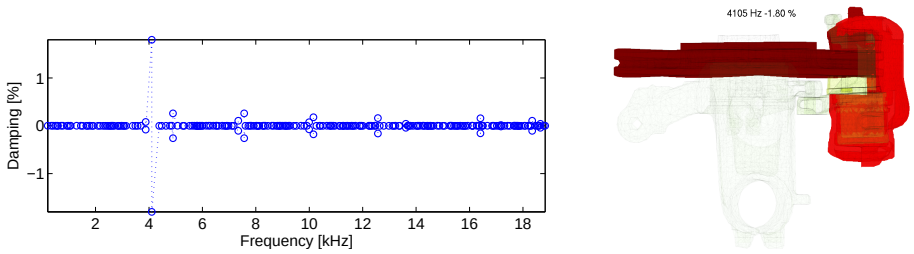

Figure 5: Left: Brake stability diagram at 12 Bar, Right: Unstable mode C44

Applying the Component Mode Tuning method, presented in [12], sensitivity of stability to component modes can be analyzed. In particular most unstable modes are sensitive (in terms of strain energy localization) to the disc, anchor and caliper, while only a few modes are sensitive to the pads.

The frequency simulation presents several unstable modes. It was shown in [6] however that unstable modes may not actually respond in a transient analysis.

3.1.2 Stability evaluation from a non linear time simulation

The non linear time simulation has the advantage of producing an actual deviation from the static response. Vibration levels can also be recovered so that noise and vibration levels can be estimated and experimental correlation is possible. Modal sensors, presented in [18] are used here to give the energy contribution of each real mode to the time response.

A time step of $10^{-6}s$ was found to produce converged results (no significant response variation when the time step is further decreased) and is therefore used here. The damping strategy to produce a working base result uses a global Rayleigh damping ratio set at 1% at $40kHz$. Modal damping [18, 19] is used in the frequency range of interest for the results provided in figure 6. None is used for the nominal simulation. Results are subsampled at $100kHz$ to allow an already fine observation.

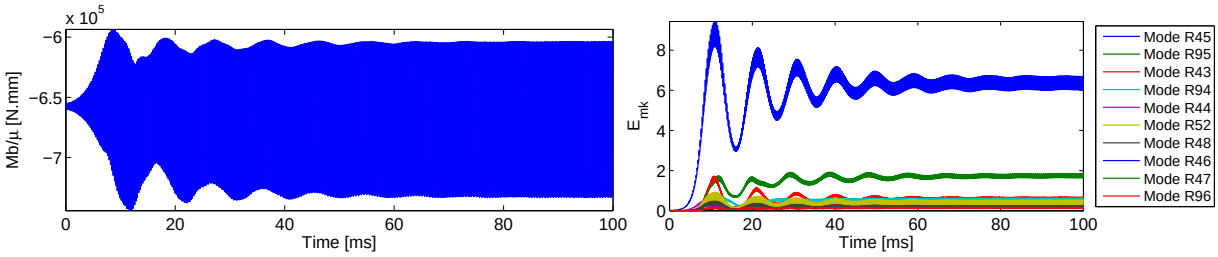

Figure 6: Squeal simulation of an industrial brake, limit cycle installation. Left: braking torque signal. Right: Modal sensors results plotted for the ranked 10 largest contributors at 100ms

With a small perturbation from the static state, the response presents a self excited divergence where energy grows without external inputs, and after a stabilization period, the response becomes nearly periodic. This is illustrated in figure 6, which presents a measure synthesizing the friction forces as the global braking torque, and figure 9 where two periods near the end of the simulation are shown.

The growth phase can be analyzed in terms of equivalent unstable poles, but the rest of the paper will focus on the nearly periodic response, which is close to a *limit cycle*. Although no attempt was made to relate the periodic response to the mathematical definition of a limit cycle, this response is fairly independent of initial conditions and is reasonably periodic. For all practical purposes, it is thus considered here as a valid *limit cycle*.

The second plot of figure 6 shows the modal sensors results. The 10 greatest modal mechanical energy values measured at 100ms are selected for the plot. The same limit cycle pattern appears, only with more details, as higher frequency modes (real mode R95 for example) responding in a significant manner can be detected. In particular, it can be observed that energy oscillations occur in the stabilized phase. Mode R45 mechanical energy (accounting for 55% of the total mechanical energy) shows a 11% mechanical energy oscillation, which will be the object of the next section.

3.2 Contact evolution and notion of dynamic stability

The mechanical energy oscillations discussed in section 3.1.2 tend to show that the system stability varies over time. Such behavior seems rather natural to explain divergence/convergence phases. The only cause of instability in the simulation presented is the friction force through its unsymmetric coupling at the pad disc interface.

Looking at the definition of tangent stiffness in equations (12) and (13), large variations can occur if the deformation amplitude becomes significant. Figures 7 and 8 plot for this purpose the contact stiffness maps for both pads. The post treatment is based on a Delaunay triangulation of the contact points at which the contact stiffness is computed. The plot is in the disc rotating plane, the rotation is clockwise, so that the disc passes from the top to the bottom in figures 7 and 8.

It is useful to note that the braking pressure is not applied in the same way for both pads. Looking at figure 3, it can be seen that the inner pad is actioned by the piston at its center while the outer pad is actioned by the caliper through two *fingers* at both sides of the pad.

The inner pad shows a 66% variation of the maximum contact stiffness under the piston while the load is more or less distributed on the pad. The disc entry side is not very loaded.

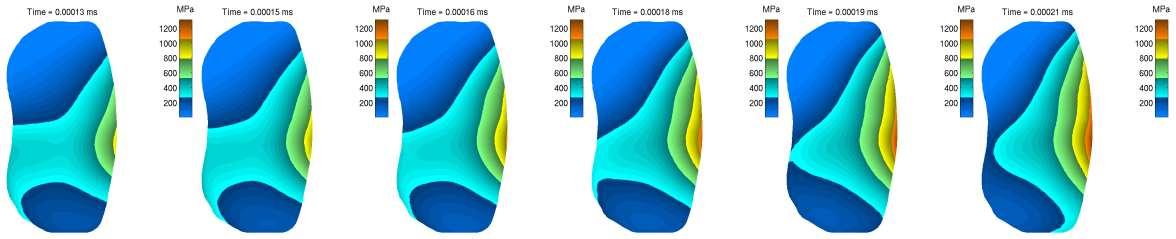

Figure 7: Contact stiffness map variation in the squeal limit cycle for the inner pad

The disc entry side of the outer pad does not vary much and remains highly loaded. The exit side however shows large variations as a slip-separation pattern occurs. This area shows then a stiffness variation from almost nothing (due to the penalization) to a rather large value (1300 MPa).

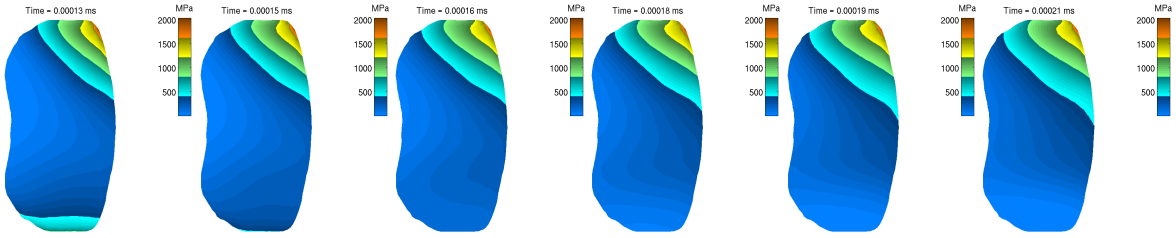

Figure 8: Contact stiffness map variation in the squeal limit cycle for the outer pad

The very large stiffness variations observed on both pads impact the tangent friction stiffness, which drives the system stability. A post-treatment is suggested here to evaluate the system stability over time. A set of deformation from the time simulation is extracted and a stability diagram is computed at each state. A *dynamic* stability diagram output from the time simulation is presented in figure 9 for the unstable modes C44, C51 and C84, along with the points taken over two limit cycles.

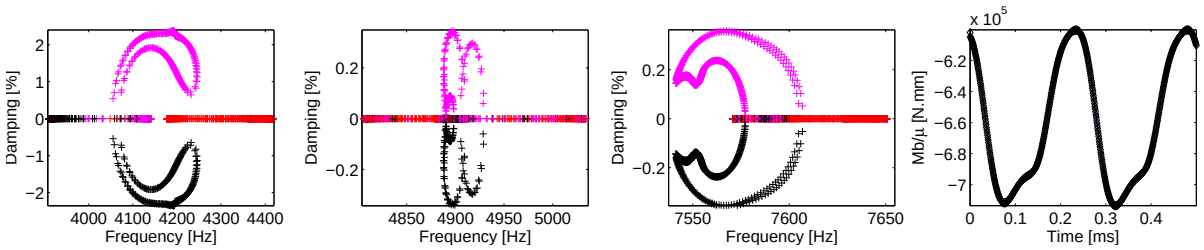

Figure 9: Dynamic stability diagrams for modes C44, C51 and C84. Right: computation points taken in the limit cycle

The complex mode stability greatly varies over time. In particular, the three most unstable modes show stable/unstable transitions. The system consequently passes through unstable states provoking energy increase and stable states provoking energy decrease.

Along with the stability variations, significant complex mode frequency variations occur as function of time. Figure 10a plots frequency variations over time at 4kHz (mode C44 frequency). It can be seen in particular that a mode shows a frequency variation of 1kHz between 3.4 and 4.4kHz.

The main instability around mode C44 can be characterized by figure 10a. It is here seen that in a limit cycle (2 cycles plotted), the complex mode C44 identified as the main instability contributor is unstable only 50% of the time. A clear interaction is besides detected between the mode crossing pattern and the stability transition pattern.

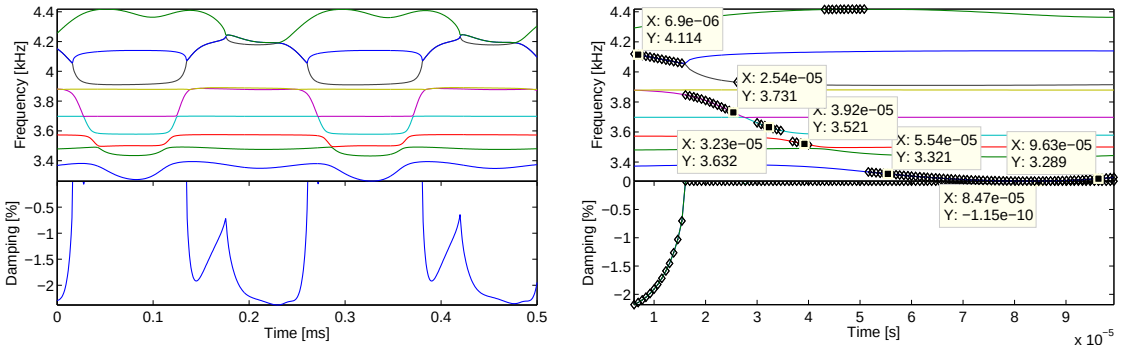

(a) Dynamic stability evolution over two cycles

(b) Varying mode shape identification points

Figure 10: *Dynamic* stability evaluation around the main instability at 4kHz

The moving shape is highly sensitive to friction coupling and is therefore thought to be mode C44 nominal shape. The shape associated to the moving mode can be identified by tracking the moving mode between the nominal frequencies. The identified points are plotted in figure 10b. Some outlying points are present due to tolerance setting difficulties when the mode crosses other modes.

The moving shape is directly mode C44 shape at the nominal state. The identified shape is then mainly based on the outer pad exit side bending. Variations occur however as movements of higher amplitude from the anchor, caliper and disc can be seen.

As function of the time deformation, the separation pattern observed softens the pad/disc contact at the outer pad exit end, lowering the unstable mode frequency and letting it transition to stability.

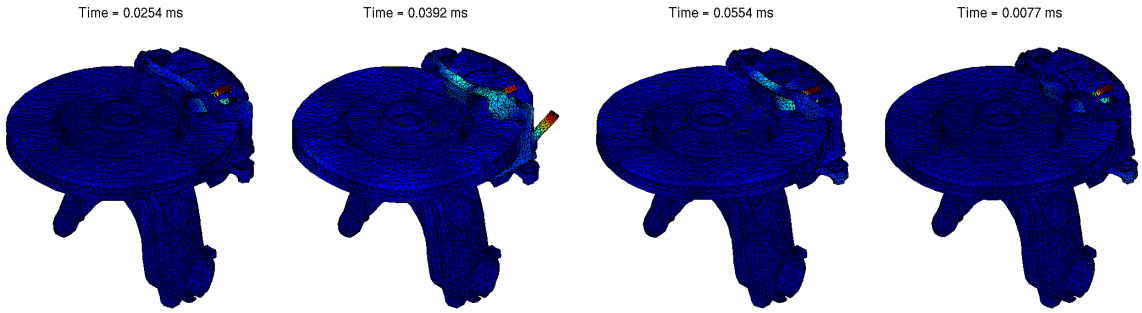

Figure 11: Identification of the shape associated to the varying mode at 4kHz

3.3 Pseudo complex mode time simulation

This section aims at trying to recover the patterns observed in an actual time simulation for a given complex mode. For a complex mode ψ_j at frequency ω_j, a pseudo-trajectory can be computed such that using an amplification factor α_j, a signal can be reconstructed

$$\begin{cases} q_{\psi_j}(t) = \Re\left(\alpha_j \psi_j e^{i\omega_j t}\right) \\ \dot{q}_{\psi j}(t) = \Im\left(\alpha_j \psi_j e^{i\omega_j t}\right) \end{cases} \tag{18}$$

The resulting signal is taken as a pseudo time simulation based on the trajectory of a complex mode. The non linear effects due to contact can be clearly observed. In particular, the slip-separation pattern due to mode C44 shape, is more or less effective (figure 12).

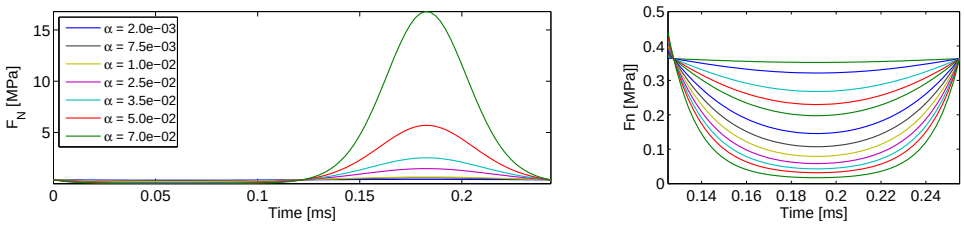

Figure 12: Slip-separation pattern observed at a sample contact point, based on mode C44 trajectory for various amplification factors

'Dynamic' stability diagrams can be computed in the same way than for a real time simulation. The results are presented in figures 13 and 14. It can be observed that the same stable/unstable transition patterns occurs. Besides, the mode crossing pattern is very depending on the amplitude factor (figure 14).

Stabilization patterns occur for relatively low amplification factors, although the mode crossing pattern is limited. As the amplification factor increases, the frequency variation gets larger so that patterns similar to figure 10a can be seen.

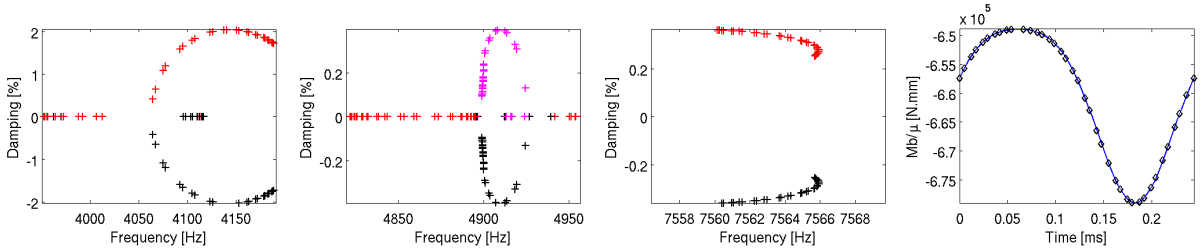

Figure 13: Pseudo dynamic stability diagrams for modes C44, C51 and C84, based on mode C44 trajectory for $\alpha_{44} = 10^{-2}$. Right: computation points taken in the pseudo limit cycle

Simulating several cycles is not relevant as the non linear effects here are only a consequence of the imposed displacement. The sustainability of a complex mode can however be tested, as its capacity to preserve its instability over its own trajectory is evaluated.

The perspective set by this section is clearly a low cost evaluation of the vibration amplitude an unstable complex mode can generate before facing stable/unstable transitions. Although exact non linear effects still require an actual time simulation for prediction accuracy, knowing in advance the critical complex modes improves initialization strategies for time simulations.

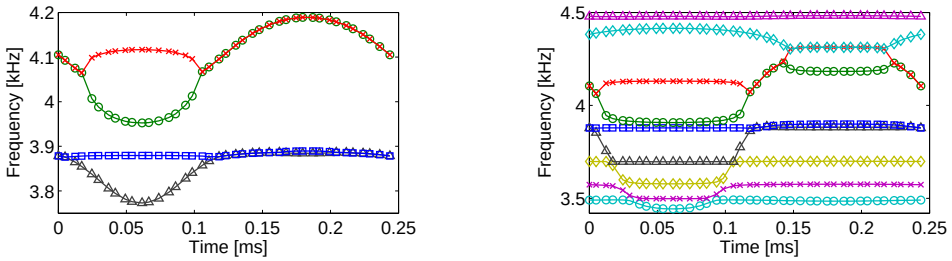

(a) $\alpha = 10^{-2}$ (b) $\alpha = 3.510^{-2}$

Figure 14: Frequency variation of the brake complex modes in the squeal limit cycle at 4kHz, based on mode C44 trajectory for two values of α

Conclusion

The work presented here is the following of [11] which aims along with [12] and [18] at implementing a design oriented time/frequency analysis of automotive brake systems. The end objective is obviously to obtain a robust design method for silent brakes, or at least with a controlled noise level.

This paper presents several contact implementations, along with the notion of tangent contact-friction states. The concepts presented can be well exploited with non linear penalized contact-friction formulations, but can also be transposed to Lagrange formulations. Experimental results greatly lack to the refinement of penalized contact-friction laws which are critical to the instability characterization.

The complex modes computed show great structural effects, as components not directly involved in the pad/disc interface show great instability sensitivity. This justifies in particular the need to simulate a complete brake assembly to characterize the instability. The system consequently features a large number of modes in the frequency range of interest, such that detecting the relevant instability along with its actual vibration level requires a time simulation.

The squeal simulation presented features a slip-separation pattern which amplitude greatly impacts the perceived contact stiffness at the pad/disc interface as function of time. The system stability thus varies over time such that mechanical energy oscillations occur in the established limit cycle. The computation of dynamic stability diagrams shows in particular that the complex mode contributing the most to the limit cycle has stable/unstable transitions, along with a large frequency vibration. This is an explanation of the energy saturation observations at the end of the divergence phase characterizing the instability.

Since complex modes are much cheaper to compute than a long time simulation, the exploitation of pseudo dynamic stability diagrams based on an unstable complex mode trajectory can be considered. The paper showed that an amplitude factor exists at which stable/unstable transition can exist. The critical amplitude at which complex mode transition occurs is then an indicator of complex mode sustainability over its own response. Low cost predictions of vibration amplitude levels could then be exploited, for early design stages, and for time simulation initialization optimization for accurate evaluation.

References

[1] M. Tan, K. Stepper, K. Abdelhamid, A.-H. Afaneh, and P. Blaschke, “An integrated process for design against brake squeal,” in *International Modal Analysis Conference (IMAC XXI)*, 2003.

[2] H. Jun and T. Gang-Feng, “Complex mode analysis on disc brake squeal and design improvement,” in *SAE paper, No. 2009-01-2101*, 2009.

[3] ABAQUS/Standard, *Theory Manual*, vol. 1. Hibbit, Karlsson, Sorhensen, Inc., 2008.

[4] P. R. Dahl, "Solid friction damping of mechanical vibrations," *AIAA Journal*, vol. 14, pp. 1675–1682, 1976.

[5] G. Chevallier, *Etude des vibrations de broutement provoquées par le frottement sec. Application aux systèmes d'embrayage*. PhD thesis, Université Paris VI Pierre et Marie Curie, 2005.

[6] X. Lorang, *Instabilité vibratoire des structures en contact frottant: Application au crissement des freins de TGV*. PhD thesis, Ecole Polytechnique, 2007.

[7] G. Kerchen, M. Peeters, J.-C. Golinval, and A. Vakakis, "Nonlinear normal modes, part i: A useful framework for the structural dynamicist," *Mechanical Systems and Signal Processing*, no. 23, pp. 170–194, 2009.

[8] M. Peeters, R. Viguié, G. Sérandour, G. Kershen, and J.-C. Golinval, "Nonlinear normal modes, part ii: Toward a practical computation using numerical continuation techniques," *Mechanical Systems and Signal Processing*, no. 23, pp. 195–216, 2009.

[9] T. Baumberger and C. Caroli, "Solid friction from stick-slip to pinning and aging," *Advances in Physics*, vol. 55, pp. 279–348, May 2006.

[10] L. Bureau, C. Caroli, and T. Baumberger, "Elasticity and onset of frictional dissipation at a non-sliding multicontact interface," in *Royal Society A: Mathematical, Physical and Engineering Sciences, 459 (2039)*, pp. 2787–2805, 2003.

[11] G. Vermot des Roches and E. Balmes, "Time simulation of squeal phenomena in realistic brake models," in *Proceedings of the International Conference on Advanced Acoustics and Vibration Engineering (ISMA)*, pp. 3007–3019, 2008.

[12] G. Vermot des Roches, J.-P. Bianchi, E. Balmes, R. Lemaire, and T. Pasquet, "Using component modes in a system design process," in *International Modal Analysis Conference (IMAC XXVIII)*, 2010.

[13] M. Géradin and D. Rixen, *Mechanical Vibrations. Theory and Application to Structural Dynamics.* John Wiley & Wiley and Sons, 1994, also in French, Masson, Paris, 1993.

[14] M. Géradin and A. Cardona, "Time integration of the equations of motion in mechanism analysis," *Computers & Structures*, vol. 33, no. 3, pp. 801–820, 1989.

[15] J. Baumgarte, "Stabilization of constraints and integrals of motion in dynamical systems," *Computer methods in Applied Mechanics and Engineering*, 1972.

[16] M. Hulbert and T. Hughes, "Space-time finite element methods for second-order hyperbolic equations," *Computer methods in Applied Mechanics and Engineering*, no. 84, pp. 327–348, 1990.

[17] T. Hughes, "Stability, convergence and growth and decay of energy of the average acceleration method in nonlinear structural dynamics," *Computers & Structures*, vol. 6, pp. 313–324, 1976.

[18] G. Vermot des Roches, E. Balmes, R. Lemaire, and T. Pasquet, "Designed oriented time/frequency analysis of contact friction instabilities in application to automotive brake squeal," in *Vibrations, Chocs & Bruit (VCB XVIIth symposium)*, 2010.

[19] J.-P. Bianchi, E. Balmes, G. Vermot des Roches, and A. Bobillot, "Using modal damping for full model transient analysis," in *Proceedings of the International Conference on Advanced Acoustics and Vibration Engineering (ISMA)*, 2010.